nature climate change

Article

https://doi.org/10.1038/s41558-023-01738-w

Climate intervention on a high-emissions pathway could delay but not prevent West Antarctic Ice Sheet demise

Received: 25 June 2022

Accepted: 20 June 2023

Published online: 10 August 2023

Check for updates

J. Sutter[1,2] ✉, A. Jones[3], T. L. Frölicher[1,2], C. Wirths[1,2] & T. F. Stocker[1,2]

Solar radiation modification (SRM) is increasingly discussed as a tool to reduce or avert global warming and concomitantly the risk of ice-sheet collapse, as is considered possible for the West Antarctic Ice Sheet (WAIS). Here we analyse the impact of stratospheric aerosol injections on the centennial-to-millennial Antarctic sea-level contribution using an ice-sheet model. We find that mid-twenty-first-century large-scale SRM could delay but ultimately not prevent WAIS collapse in a high-emissions scenario. On intermediate-emissions pathways, SRM could be an effective tool to delay or even prevent an instability of WAIS if deployed by mid-century. However, SRM interventions may be associated with substantial risks, commitments and unintended side effects; therefore, emissions reductions to prevent WAIS collapse seem to be the more practical and sensible approach at the current stage.

The notion of offsetting global warming by means of solar climate intervention, or solar radiation modification (SRM), is at the centre of an intense debate on the intrinsic governance dilemma[1–3]. Stratospheric aerosol deposition, the injection of particles reflecting incoming solar radiation into the stratosphere as a means to limit global warming, is one form of SRM. Substantial SRM interventions promise, in theory, to stop global warming quasi-instantaneously[4,5] and at relatively limited cost[6,7]. The door to limit climate warming to well below 2 °C via greenhouse gas mitigation within the twenty-first century is rapidly closing[8,9]. As every decade of delayed emissions reduction increases the committed warming[10], SRM interventions might be seriously considered in the future.

While the effectiveness of SRM to halt anthropogenic climate change has been quantified by modelling studies[11–13], the regional impacts of planetary SRM remain highly uncertain[14]. This is due to an insufficient understanding of the responses of the hydrological cycle[14] and atmospheric chemistry[4] to such interventions. Potential side effects of SRM range from shifting monsoon patterns[15] to changes in the meridional temperature gradients[16], in atmospheric and oceanic circulations[17,18] and in the statistics of the modes of climate variability[18], all of which are insufficiently studied[3]. In summary, SRM could have impacts on regional weather patterns detrimental to society and the biosphere[19–21], and other still-unknown effects, while not addressing the direct adverse effects of rising atmospheric CO_2 such as ocean acidification[22]. Furthermore, the effect of SRM on the polar ice sheets remains largely unexplored.

SRM research to date has been confined to model simulations and laboratory studies. Field experiments that mimic natural analogues such as volcanic eruptions (for example, the Stratospheric Controlled Perturbation Experiment[23]) have encountered societal and political barriers to deployment. The physical, governance and ethical challenges of SRM interventions to combat anthropogenic climate change continue to be publicly debated[3,24]. Issues concern the risk of delaying (or even inhibiting) mitigation efforts, unilateral deployment of SRM, termination shock[25] and intergenerational injustice[2]. One premise of SRM interventions would be to prevent the triggering of tipping points[26,27] in the climate system, such as a potential marine ice-sheet instability of the West Antarctic Ice Sheet (WAIS) through self-sustained grounding-line retreat[28] assuming that it is not under way already[29].

Numerous studies are dedicated to the question whether the observed grounding-line retreat in West Antarctica is due to an ongoing marine ice-sheet instability[30] or simply a response to current

[1]Climate and Environmental Physics, Physics Institute, University of Bern, Bern, Switzerland. [2]Oeschger Centre for Climate Change Research, University of Bern, Bern, Switzerland. [3]Met Office, Exeter, UK. ✉e-mail: johannes.sutter@unibe.ch

https://doi.org/10.1038/s41558-023-01738-w

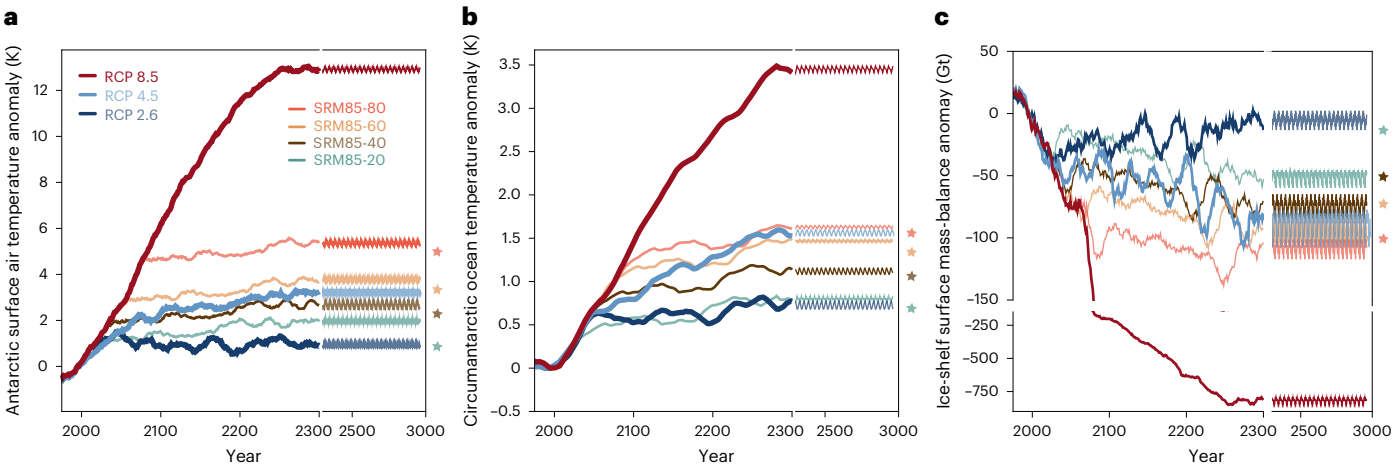

Fig. 1 | Simulated changes of Antarctic climate conditions in response to GHG emissions and solar climate intervention scenarios. a, Antarctic surface air temperature anomalies for RCP 2.6, RCP 4.5 and RCP 8.5 scenarios as well as for the stratospheric aerosol injection scenarios SRM85-20, -40, -60 and SRM85-80 (dashed lines). SRM45 temperatures (year 2300 and beyond) are depicted by stars next to time series. **b**, Same as **a** but for circumantarctic (ice front) Southern Ocean subsurface (400–700 m) temperature anomalies. **c**, Antarctic ice-shelf surface mass-balance anomalies. Note the shift in the time axis at the year 2300 in all panels and the shift in *y* axis in panel **c** at −150 Gt. All values are relative to the historical period 1995–2014 and 20 yr running average. From year 2300 onwards, the forcing from 2270 to 2300 is continuously repeated.

ocean variability and the resulting ice-shelf mass-balance anomalies[31]. Answering this question is challenging due to the intrinsic uncertainties of ice-sheet models[32] and the applied climate forcing[33]. It is definite that offsetting sea level would require serious emissions-mitigation efforts[34]; however, it is unclear whether grounding lines in West Antarctica might continue retreating even under current climate conditions[35,36]. A lack of progress on decarbonizing the economy and society could potentially lead to substantial ice-sheet loss and multi-metre sea-level rise on centennial timescales due to melting of glaciers, the Greenland Ice Sheet and the Antarctic Ice Sheet (AIS) and ocean thermal expansion[37,38]. Considering the severe physical, ecological and societal disruptions caused by sea-level rise, pressure could be mounting to employ some form of SRM on a global, regional or local scale sometime during the twenty-first century.

However, the literature so far available on the impact of SRM on the polar ice sheets is very limited[39] and restricted mostly to the analysis of atmospheric and oceanic conditions in and around Greenland and Antarctica[17,40–42]. To our knowledge, explicit ice dynamic modelling studies under SRM scenarios for Antarctica do not yet exist, while more unconventional climate intervention ideas, such as artificial mass deposition in West Antarctica[43] or building subsea walls blocking warm ocean currents[44], have been investigated.

In this Article, we investigate the long-term response of the AIS in a geoengineered future compared with a low-emissions strong-mitigation (representative concentration pathway (RCP) 2.6), an intermediate-emissions stabilization (RCP 4.5) and a high-emissions no-mitigation (RCP 8.5) scenario. We are aware that the high-emissions no-mitigation scenario paints a rather pessimistic picture of future GHG emissions as current climate policies are more congruent with the RCP 4.5 scenario, and emissions-mitigation pledges even leave a chance to stay within 2 °C warming[8]. However, it is sensible to assume that RCP 8.5 is a scenario under which SRM interventions would be seriously considered.

We employ the Parallel Ice Sheet Model (PISM[45]) in a range of parameterizations (Extended Data Table 1) and at 16 (default configuration), 8 and 4 km grid resolution (Extended Data Fig. 1). PISM is forced with previously produced[11] output from the global coupled Hadley Centre Global Environmental Model Version 2 (HadGEM2-ES) under three different representative concentration scenarios spanning the range of plausible emissions pathways (RCP 2.6, RCP 4.5 and RCP 8.5) and four SRM climate scenarios (Fig. 1) and extended to the year 2300 for this study. We consider four different starting dates of stratospheric aerosol injections under the RCP 8.5 scenario, either in the year 2020 or later in 2040, 2060 and 2080, henceforth called SRM85-20, -40, -60, -80, with equivalent nomenclature used for SRM under the RCP 4.5 scenario. After the year 2300 (end of HadGEM2-ES simulations), we repeat the last 30 years of each simulation output until the year CE 3000 (an in-depth description of climate forcing and ice-sheet model set-up is provided in Methods).

Antarctic climate forcing under RCP scenarios

In the high-emissions scenario RCP 8.5, Antarctic surface air temperature anomalies (with respect to the period 1995–2014) peak around 13 °C (Fig. 1a) in the year 2300. A southward shift of the westerly winds associated with increased ocean upwelling (Extended Data Figs. 2 and 3) combined with warming of the subsurface circumantarctic Southern Ocean (adjacent to calving or ice front, averaged over 400–700 m depth) leads to 1 °C and 3.5 °C warmer ocean waters around the Antarctic continent by the years 2100 and 2300, respectively (Fig. 1b). Widespread surface melt above the Ross and Filchner–Ronne ice shelves occurs within the second half of the twenty-first century under RCP 8.5, dominating the overall Antarctic negative surface mass balance (Fig. 1c). Locally, surface melt occurs on the grounded parts of the ice sheet after 2100 as well. By contrast, neither RCP 4.5 nor RCP 2.6 shows sustained surface melt by the year 2300. However, subsurface Southern Ocean warming in RCP 4.5 is twice as large as in RCP 2.6 (1.5 °C versus 0.7 °C) in 2300, and the global surface air temperature anomaly reaches 3 °C (year 2300). In all scenarios, the subsurface Southern Ocean continues to warm in the year 2300, albeit at a reduced pace (Fig. 1b).

Persistent Southern Ocean warming despite climate stabilization

Instantaneous deployment of a planetary-scale SRM in the year 2020 (SRM85-20) leads to an almost immediate (after a few years) levelling of the mean Antarctic surface air temperature anomaly below 2 °C, but the subsurface ocean warming by about 0.5 °C (similarly to RCP 2.6) continues until 2050, after which ocean temperatures only slowly increase until the year 2300 (Fig. 1b). Likewise, in RCP 2.6, the surface air temperature anomaly does not exceed 2 °C global warming, with a long-term stabilization around 1.5 °C until the year 2300. Overall, the

climatic drivers relevant for the AIS in SRM85-20, SRM45-20 and RCP 2.6 are almost identical with the exception of a slightly lower ice-shelf surface mass balance and slightly warmer surface air temperature in SRM85-20 (Fig. 1a,c). However, intermittent regional ocean temperature difference between RCP 2.6 and SRM85-20 can be as high as 1.0–1.5 °C (Supplementary Fig. 4). Importantly, we do not observe increased ocean upwelling and associated changes in temperature in the Southern Ocean under the SRM scenarios, in contrast to a previous study[40] (Supplementary Note 1).

While the warming of the subsurface Southern Ocean until the year 2300 in SRM85–60/80 is very similar to that in RCP 4.5, the surface air temperature in SRM85–60/80 is higher than under RCP 4.5, resulting in a more negative surface mass balance of the Antarctic ice shelves (Fig. 1c). It is important to note that HadGEM2-ES ranks among the more-sensitive models in the Coupled Model Intercomparison Project Phase 5 (CMIP5) ensemble with respect to both ocean warming and Antarctic surface mass balance[46]. However, the negative surface mass-balance anomalies computed in HadGEM2-ES for the end of the twenty-first century are comparable to recent estimates from a regional climate model[47] in both magnitude and spatial patterns (Extended Data Fig. 4; see also Supplementary Note 2 for a discussion of future surface mass-balance changes). We consider this a feature of our forcing as in reality SRM interventions would most likely be considered on a high climate sensitivity trajectory, that is, in a world in which severe climate impacts materialize sooner.

Antarctic ice loss under RCP 8.5

Under RCP 8.5, the collapse of the WAIS is well under way by the year 2300 (Fig. 2). The individual contribution of the WAIS to sea-level rise amounts to 0.3–0.8 m (see Fig. 2a), and that of the entire AIS is 0.6–1.1 m (Fig. 2b and Extended Data Table 2). This is due to the surface-melt-induced loss of both the Ross and Filchner–Ronne ice shelves and the rapid retreat of Thwaites glacier in response to the ocean thermal forcing in the Amundsen Sea sector. It is important to note that, while ice-sheet retreat and sea-level contribution by the year CE 3000 (WAIS: 2.1–2.8; AIS: 2.9–4.0 m; Fig. 2a,b and Extended Data Table 2) are largely independent of the grid resolutions applied here, the timing of Thwaites collapse is not (Extended Data Fig. 5).

At 16 km horizontal resolution, the inroad to WAIS collapse in RCP 8.5 begins with the collapse of the Ross Ice Shelf, only then followed by retreat of the Thwaites grounding line. This is in response to the widespread surface melt above the Ross Ice Shelf in the second half of the twenty-first century, leading to the loss of the whole ice shelf and subsequent acceleration of the major Ross-sector ice streams (Fig. 3e,f). Thus, the collapse of Thwaites is rather a secondary response to the rapid retreat opposite of the WAIS ice divide and ongoing drawdown of the WAIS surface elevation. This suggests a drainage-basin-scale interaction of a marine ice-sheet instability (MISI in one basin triggering MISI in a neighbouring basin) as discussed earlier[48].

By contrast, at 4 and 8 km resolutions, the collapse of Thwaites Glacier is initiated much earlier as the ice-sheet model response to elevated ocean temperatures is more pronounced. The retreat is initially confined to the Amundsen Sea Embayment and subsequently engulfs the whole WAIS. Here we consider an ice-sheet model ensemble that is consistent with the model sensitivity highlighted in Ice Sheet Model Intercomparison Project for CMIP6 (Supplementary Fig. 5).

In East Antarctica, the Wilkes Basin grounding line along the George V coast remains stable; that is, there is no ongoing forced or self-sustained retreat until the year CE 3000 independent of the emissions scenario (Fig. 3e,f). This is despite mass loss from this drainage sector. The stability of the George V coast grounding line is robust in all tested resolutions (16, 8 and 4 km) and in agreement with a recent high-resolution study determining the ice sheet's future response after complete loss of ice-shelf buttressing force[49], as well as another study constraining its dynamics during the Last Interglacial[50]. However, we note that in the pre-industrial control simulations, ice cover along the George V coast is elevated compared with observations (Supplementary Fig. 8). This means that the modelled response might underestimate ice loss in this region.

Totten Glacier is retreating, and the glaciers of the Recovery Basin are losing mass rapidly (Fig. 3e,f). However, under RCP 8.5, mass gains (~0.2–0.3 m sea-level-equivalent ice volume) in Dronning Maud Land and central East Antarctica (~0.4–0.5 m, respectively) partly compensate for grounding-line retreat in East Antarctica. Interestingly, the substantial grounding-line retreat of the Recovery, Bailey and Slessor glaciers is balanced by mass gains in the hinterland of these glaciers.

In RCP 8.5, Antarctica contributes 3.2–4.0 m to global sea level by the year CE 3000 (Fig. 2b and Extended Data Table 2) and still loses mass at a rate 5–10 times faster than observed today (Fig. 2d and Supplementary Fig. 6). According to our simulations, the impact of runaway climate change on Antarctic ice-mass change will be discernible from mitigation or SRM scenarios only by the second half of the twenty-first century. Its imprint on global sea level diverges even later (Fig. 2a,b), in agreement with recent model estimates[51,52] but contrasting studies where hydrofracturing and cliff failure are considered[53]. We find that for both RCP 8.5 and RCP 4.5, WAIS collapse is irreversible; that is, there is no recovery on millennial timescales (Supplementary Note 3 and Supplementary Figs. 2 and 3).

Ice-sheet stability under rapid decarbonization or early SRM

The only scenarios mostly ensuring WAIS stability (absence of MISI or ongoing grounding-line retreat) are RCP 2.6 (76% of ensemble members) and early SRM interventions, meaning planetary SRM intervention starting in either the year 2020 (RCP 8.5; Fig. 2a,e) or the year 2040 (RCP 4.5; Fig. 4b). This is not surprising as the climatic drivers in RCP 2.6 and SRM85-20 are very similar. However, despite the strong emissions reductions in RCP 2.6 or the stabilization of global temperatures in SRM85-20, the subsurface circumantarctic ocean has a committed warming of an additional 0.5–0.7 °C by 2300 (regionally, this warming can reach 1.0–1.5 °C; Supplementary Fig. 4).

In the few model runs in which Thwaites Glacier is already close to or beyond a tipping point today, that is, a configuration in which a self-sustained unforced retreat of the grounding line ensues, this warming can be sufficient to trigger WAIS collapse under several parameter sets considered here. This explains the high-end tail of AIS sea-level contributions in RCP 2.6 (1.38 m) and SRM85-20 (1.08 m) by the year CE 3000 (Fig. 2a,e). Ocean temperatures in the Amundsen, Weddel and Ross seas are up to 0.5, 1.0 and 1.5 °C warmer during the middle twenty-first century (Supplementary Fig. 4), which could be one factor behind the higher sea-level range in RCP 2.6.

WAIS collapse in lower-emissions/early SRM scenarios unfolds via the disintegration of Thwaites Glacier associated with accelerating grounding-line retreat in the coming centuries. Both the Filchner–Ronne and Ross ice shelves remain intact during the next centuries in the SRM85-20, RCP 2.6 and RCP 4.5 scenarios; thus, the only path towards WAIS collapse is due to elevated basal melt underneath the ice shelves of the Amundsen Sea sector. Importantly, the chances of WAIS collapse in SRM85-20 and RCP 2.6 are nearly identical, with very similar median long-term sea-level contributions (~0.50 and 0.75 m by the year CE 3000, respectively). Notably, while some simulations in the ensemble do project negative sea-level contributions for RCP 2.6 and SRM85-20, those matching the historical record do not.

SRM in a middle-of-the-road scenario

Current decarbonization policies and actions correspond to a middle-of-the-road scenario resulting in warming of global temperatures by ~2.8 °C by the end of this century[54]. We investigate the impact of a continuous SRM intervention under the RCP 4.5 scenario following the same approach as in the case of RCP 8.5 (employment in 2020, 2040,

https://doi.org/10.1038/s41558-023-01738-w

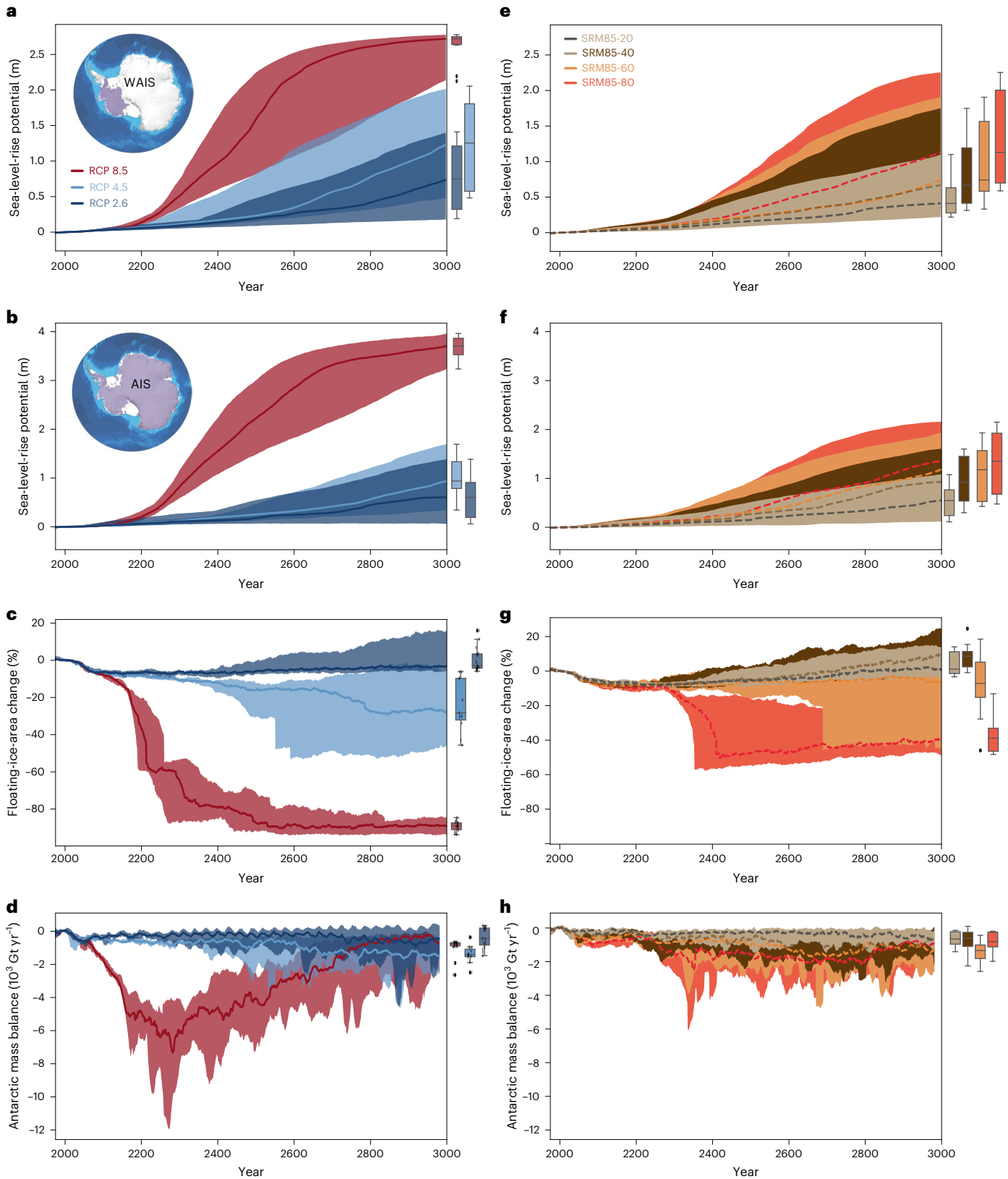

Fig. 2 | WAIS and AIS response to GHG emissions and solar climate intervention scenarios. a,**e**, West Antarctic sea-level-equivalent ice-volume change (median and standard deviation) in the scenarios RCP 2.6, RCP 4.5 and RCP 8.5 (**a**) as well as SRM85-20, -40, -60 and -80 (**e**). **b**,**f**, AIS sea-level-equivalent ice-volume change (median and minimum/maximum ensemble members) in the RCP scenarios (**b**) as well as SRM85 scenarios (**f**). **c**,**g**, AIS change in ice-shelf area (relative to 1993–2017) in the RCP scenarios (**c**) as well as SRM85 scenarios (**g**). **d**,**h**, Annual Antarctic ice loss in gigatonnes in the RCP scenarios (**d**) as well as SRM85 scenarios (**h**). All time series shown as 20 yr running mean. Box plots next to panels illustrate the statistical distribution (17 ensemble members) at the year CE 3000 with median (black line) and interquartile range of ensemble (box); whiskers extend to the farthest ensemble member within 1.5 times the interquartile ensemble range (outliers are depicted by black dots).

https://doi.org/10.1038/s41558-023-01738-w

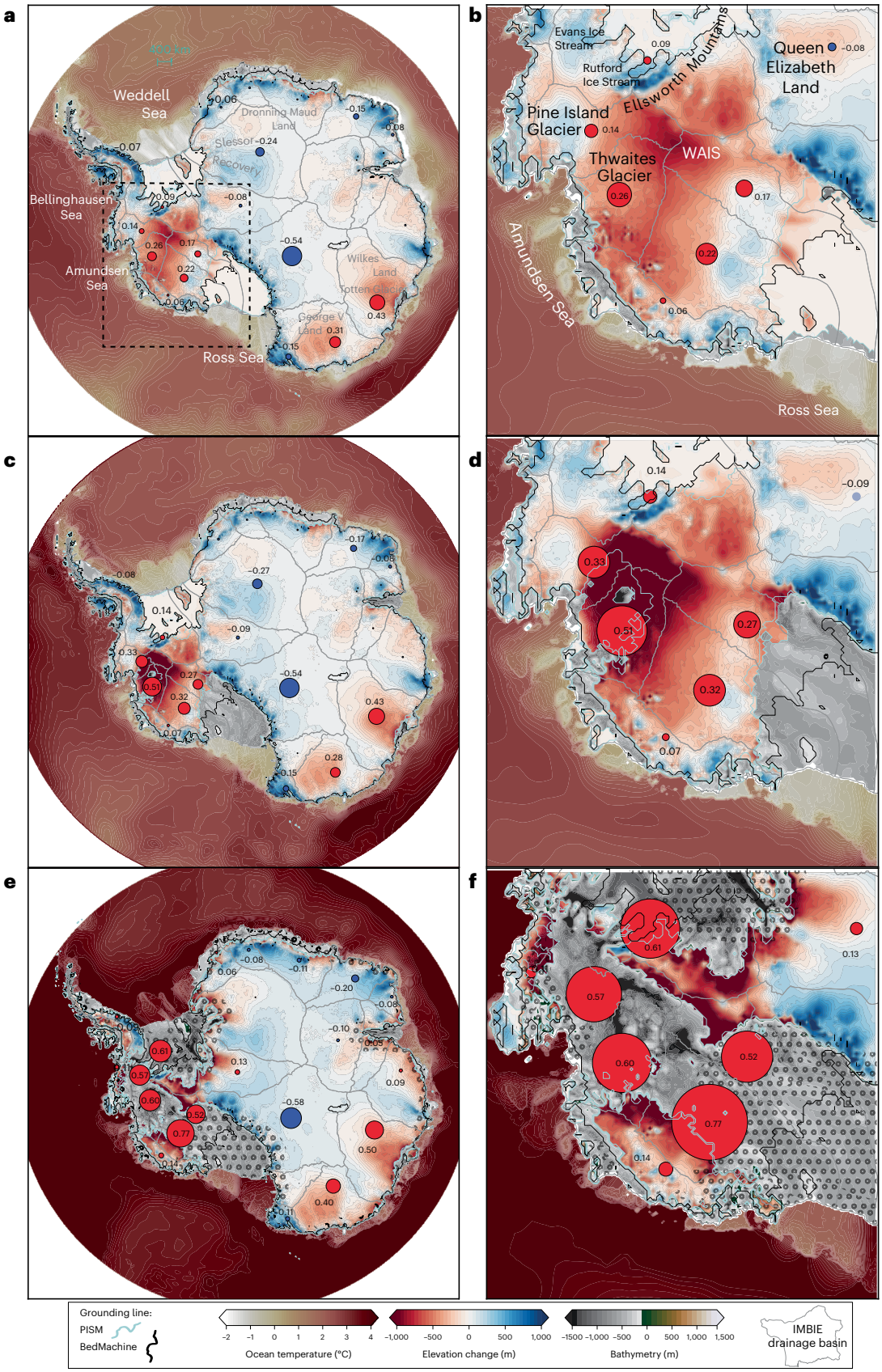

Fig. 3 | AIS and WAIS in the year CE 3000 under different GHG emissions scenarios. a,**c**,**e**, Change in AIS elevation (colours) and the corresponding sea-level contribution (numbers in units of metres) of the different Antarctic drainage sectors as well as ocean subsurface temperatures for RCP 2.6 (**a**), RCP 4.5 (**c**) and RCP 8.5 (**e**). **b**,**d**,**f**, Enlarged view of the WAIS for RCP 2.6 (**b**), RCP 4.5 (**d**) and RCP 8.5 (**f**). Elevation changes are computed against the present-day ice sheet from BedMachine Antarctica[59,60]. Coloured circles display the regional sea-level contribution of individual catchment areas. Dotted areas in all panels highlight regions experiencing surface melt. Drainage sectors (delineations based on ice provenance) are depicted by thin grey lines[61].

https://doi.org/10.1038/s41558-023-01738-w

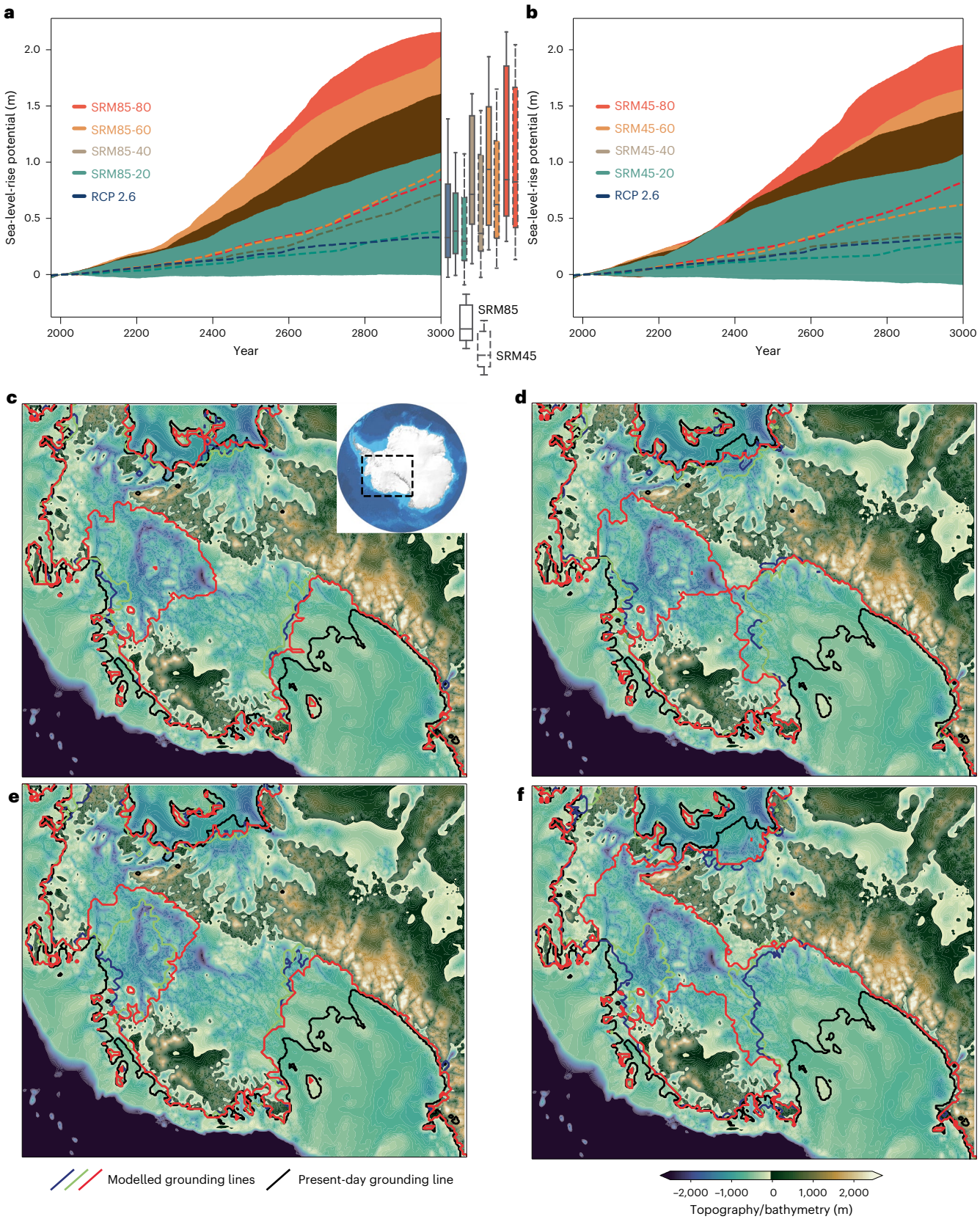

Fig. 4 | Antarctic sea-level contribution and grounding-line migration in SRM85 compared with SRM45. a,**b**, Antarctic sea-level-equivalent ice-volume changes in the scenarios SRM85-20, -40, -60, -80 (**a**) and SRM45-20, -40, -60, -80 (**b**). Thick dashed lines depict ensemble median, and box plots show median (black line) and interquartile range of ensemble (17 ensemble members), and whiskers extend to the farthest ensemble member within 1.5 times the interquartile ensemble range. Box plots with dashed outline correspond to the SRM45 scenarios. **c**–**f**, West Antarctic grounding-line positions in three selected model realizations for SRM45-40 (**c**) SRM45-80 (**d**), SRM85-40 (**e**) and SRM85-80 (**f**) in the year CE 3000 (coloured lines). Black line depicts present-day observed grounding line[59,60]. Bathymetry/topography plotted for reference in the background[59,60].

https://doi.org/10.1038/s41558-023-01738-w

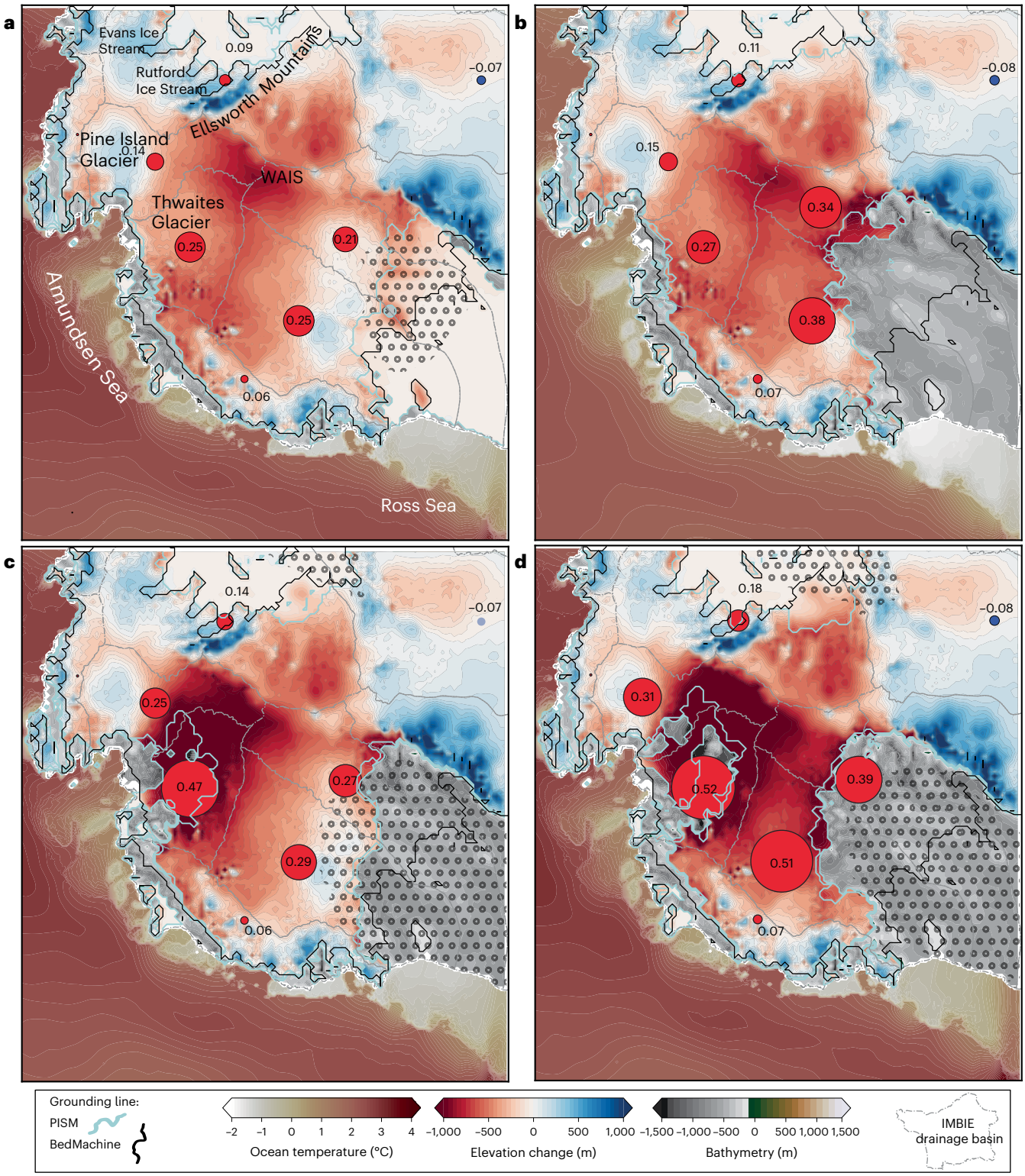

Fig. 5 | WAIS in the year CE 3000 under different SRM scenarios. a, SRM45-60. **b**, SRM45-80. **c**, SRM85–60. **d**, SRM85-80. Colours depict the change in Antarctic ice-sheet elevation, and numbers represent the corresponding sea-level contribution (in metres) of Antarctic drainage sectors; ocean subsurface temperatures are also depicted. Elevation changes are computed against the present-day ice sheet from BedMachine Antarctica[59,60]. Coloured circles display the regional sea-level contribution of individual catchment areas. Dotted areas in all panels highlight regions experiencing surface melt. Drainage sectors (delineations based on ice provenance) are depicted by thin grey lines[61].

2060 and 2080; in the case of SRM4.5, SO_2 emissions are two-thirds lower compared with SRM8.5 by the end of the twenty-first century as shown in Supplementary Fig. 7). Surprisingly, the committed ice loss until the year CE 3000 is very similar to the high-emissions pathway in case of a late intervention (2080; red dashed line in Fig. 4b,d,f). However, most ensemble members (65%) suggest a stabilization of the grounding line under SRM45-40 (SRM started in 2040), whereas a long-term collapse is triggered for SRM85-40 in 70% of the simulations.

This indicates that WAIS collapse might be prevented by SRM under an RCP 4.5 scenario even for mid-century interventions, however with a substantial risk of failure (35%).

Committed ice-sheet collapse despite climate intervention

Delay of SRM85 by 20, 40 or 60 years increases both the committed Southern Ocean warming (Fig. 1b) and surface melt above the Ross Ice Shelf and therefore the probability of WAIS collapse (70%, 76%, 82%; Fig. 4). Maximum (median) sea-level contributions in these scenarios amount to 1.6 (0.9) m, 1.9 (1.2) m and 2.2 (1.4) m, respectively. Moreover, if SRM is started in the year 2060, widespread surface melt over the Ross Ice Shelf is already present (Fig. 5), resulting in collapse of the ice shelf and loss of buttressing. If WAIS collapse is already triggered, the SRM intervention would have to reverse, not merely halt, climate warming due to the nonlinear increase in ice loss and hysteresis effects of the ice sheet[55] (Supplementary Figs. 1 and 2). Already in RCP 4.5, thus under current climate policies, the chance of long-term WAIS stability is reduced to a third of the ensemble members, and employment of SRM in the second half of this century mostly fails to prevent the long-term demise of the WAIS.

Discussion

Our simulations suggest that the most effective path to prevent total long-term WAIS collapse is rapid decarbonization or, depending on GHG emissions, the early deployment of planetary SRM. The latter is politically challenging and associated with unintended and potentially damaging side effects. We believe that a robust understanding of the regional impacts of planetary SRM, or any kind of climate intervention, is imperative before considering large-scale employment. Thus, at the current stage, we suggest that the best chance to guarantee the long-term stability of the WAIS is to reduce GHG emissions to net zero with no delay, thereby keeping the goal of the Paris Agreement[56] to limit global warming to well below 2 °C in reach. While in the worst-case emissions scenario (RCP 8.5) WAIS collapse and East Antarctic Ice Sheet retreat are unavoidable according to our model simulations, even RCP 4.5 would lead to a high chance of a long-term demise of WAIS. This committed retreat could be slowed should SRM interventions as considered here materialize during the twenty-first century, providing a larger time window for adaptation measures. We use a stand-alone ice-sheet model; interactive coupling to a climate model or a different model initialization would affect the timing of ice-sheet tipping and pacing of retreat. Refer to Methods and Supplementary Information for an in-depth discussion of caveats associated with our modelling choices such as parameterization, model spin-up, climate forcing and mismatches with respect to present-day observations (for example, Supplementary Notes 4 and 5).

It is important to note that we have not considered the possibility of reversing temperature conditions under high-emissions scenarios[4]. Reducing Antarctic surface and subsequently ocean temperatures via SRM after surpassing a certain climate threshold (2 °C) during the twenty-first century could further delay the demise of the WAIS. Limited polar SRM interventions[57] combined with strong emissions-mitigation policies that aim at preventing the tipping of the WAIS would be an additional modelling scenario. However, this requires more elaborate model set-ups and preferably interactive coupling between the ice sheet and the climate system. However, as long as atmospheric GHG concentrations remain high, SRM would most likely have to be continued for centuries[58], perhaps even millennia, to avoid WAIS collapse. This would be an intergenerational commitment whose cost and risks, for example due to permanent changes in the lower stratosphere and the danger of termination shock, are potentially immense but difficult to quantify. Our simulations show, in agreement with previous studies, that the impact of the adopted emissions pathways on the future AIS mass imbalance will not be discernible within this century. However, the longer actions towards limiting global warming are delayed, be it via emissions mitigation and/or SRM, the more likely a collapse of WAIS will become.

Online content

Any methods, additional references, Nature Portfolio reporting summaries, source data, extended data, supplementary information, acknowledgements, peer review information; details of author contributions and competing interests; and statements of data and code availability are available at https://doi.org/10.1038/s41558-023-01738-w.

References

1. Keith, D. W. Toward constructive disagreement about geoengineering. *Science* **374**, 812–815 (2021).
2. Biermann, F. et al. Solar geoengineering: the case for an international non-use agreement. *Wiley Interdescip. Rev. Clim. Change* **13**, e754 (2022).
3. *Reflecting Sunlight: Recommendations for Solar Geoengineering Research and Research Governance* (National Academies Press, 2021).
4. Tilmes, S. et al. Reaching 1.5 and 2.0 °C global surface temperature targets using stratospheric aerosol geoengineering. *Earth Syst. Dyn.* **11**, 579–601 (2020).
5. Tilmes, S. et al. Effects of different stratospheric SO_2 injection altitudes on stratospheric chemistry and dynamics. *J. Geophys. Res. Atmos.* **123**, 4654–4673 (2018).
6. Reynolds, J. L., Parker, A. & Irvine, P. Five solar geoengineering tropes that have outstayed their welcome. *Earths Future* **4**, 562–568 (2016).
7. Smith, W. & Wagner, G. Stratospheric aerosol injection tactics and costs in the first 15 years of deployment. *Environ. Res. Lett.* **13**, 124001 (2018).
8. Meinshausen, M. et al. Realization of Paris Agreement pledges may limit warming just below 2 °C. *Nature* **604**, 304–309 (2022).
9. Stocker, T. F. The closing door of climate targets. *Science* **339**, 280–282 (2013).
10. Allen, M. R. & Stocker, T. F. Impact of delay in reducing carbon dioxide emissions. *Nat. Clim. Change* **4**, 23–26 (2014).
11. Jones, A. C. et al. Regional climate impacts of stabilizing global warming at 1.5 K using solar geoengineering. *Earths Future* **6**, 230–251 (2018).
12. Keller, D. P., Feng, E. Y. & Oschlies, A. Potential climate engineering effectiveness and side effects during a high carbon dioxide-emission scenario. *Nat. Commun.* **5**, 3304 (2014).
13. Pinto, I., Jack, C., Lennard, C., Tilmes, S. & Odoulami, R. C. Africa's climate response to solar radiation management with stratospheric aerosol. *Geophys. Res. Lett.* **47**, e2019GL086047 (2020).
14. Tilmes, S. et al. The hydrological impact of geoengineering in the Geoengineering Model Intercomparison Project (GeoMIP). *J. Geophys. Res. Atmos.* **118**, 11036–11058 (2013).
15. Russotto, R. D. & Ackerman, T. P. Changes in clouds and thermodynamics under solar geoengineering and implications for required solar reduction. *Atmos. Chem. Phys.* **18**, 11905–11925 (2018).
16. Fasullo, J. T. et al. Persistent polar ocean warming in a strategically geoengineered climate. *Nat. Geosci.* **11**, 910–914 (2018).
17. Cheng, W. et al. Changes in Hadley circulation and intertropical convergence zone under strategic stratospheric aerosol geoengineering. *NPJ Clim. Atmos. Sci.* **5**, 32 (2022).
18. Xie, M. D., Moore, J. C., Zhao, L. Y., Wolovick, M. & Muri, H. Impacts of three types of solar geoengineering on the Atlantic meridional overturning circulation. *Atmos. Chem. Phys.* **22**, 4581–4597 (2022).
19. Ricke, K., Ivanova, D., McKie, T. & Rugenstein, M. Reversing Sahelian droughts. *Geophys. Res. Lett.* **48**, 2021GL093129 (2021).

20. Haywood, J. M., Jones, A., Bellouin, N. & Stephenson, D. Asymmetric forcing from stratospheric aerosols impacts Sahelian rainfall. *Nat. Clim. Change* **3**, 660–665 (2013).
21. Jones, A. C. et al. Impacts of hemispheric solar geoengineering on tropical cyclone frequency. *Nat. Commun.* **8**, 1382 (2017).
22. Jens, T., Thomas, L. F. & Fortunat, J. Ocean acidification in emission-driven temperature stabilization scenarios: the role of TCRE and non-CO_2 greenhouse gases. *Environ. Res. Lett.* **18**, 024033 (2023).
23. Dykema, J. A., Keith, D. W., Anderson, J. G. & Weisenstein, D. Stratospheric controlled perturbation experiment: a small-scale experiment to improve understanding of the risks of solar geoengineering. *Phil. Trans. R. Soc. B* **372**, 20140059 (2014).
24. Reynolds, J. L. Solar geoengineering to reduce climate change: a review of governance proposals. *Proc. R. Soc. A* **475**, 20190255 (2019).
25. Jones, A. et al. The impact of abrupt suspension of solar radiation management (termination effect) in experiment G2 of the Geoengineering Model Intercomparison Project (GeoMIP). *J. Geophys. Res. Atmos.* **118**, 9743–9752 (2013).
26. Lenton, T. M. Early warning of climate tipping points. *Nat. Clim. Change* **1**, 201–209 (2011).
27. Mckay, D. I. A. et al. Exceeding 1.5 °C global warming could trigger multiple climate tipping points. *Science* **377**, 1171–1181 (2022).
28. Rosier, S. H. R. et al. The tipping points and early warning indicators for Pine Island Glacier, West Antarctica. *Cryosphere* **15**, 1501–1516 (2021).
29. Rignot, E., Mouginot, J., Morlighem, M., Seroussi, H. & Scheuchl, B. Widespread, rapid grounding line retreat of Pine Island, Thwaites, Smith, and Kohler glaciers, West Antarctica, from 1992 to 2011. *Geophys. Res. Lett.* **41**, 3502–3509 (2014).
30. Favier, L. et al. Retreat of Pine Island Glacier controlled by marine ice-sheet instability. *Nat. Clim. Change* **4**, 117–121 (2014).
31. Jenkins, A. et al. West Antarctic Ice Sheet retreat in the Amundsen Sea driven by decadal oceanic variability. *Nat. Geosci.* **11**, 733–738 (2018).
32. Hill, E. A., Rosier, S. H. R., Gudmundsson, G. H. & Collins, M. Quantifying the potential future contribution to global mean sea level from the Filchner–Ronne basin, Antarctica. *Cryosphere* **15**, 4675–4702 (2021).
33. Mottram, R. et al. What is the surface mass balance of Antarctica? An intercomparison of regional climate model estimates. *Cryosphere* **15**, 3751–3784 (2021).
34. Seroussi, H. et al. ISMIP6 Antarctica: a multi-model ensemble of the Antarctic ice sheet evolution over the 21st century. *Cryosphere* **14**, 3033–3070 (2020).
35. Reese, R. et al. The stability of present-day Antarctic grounding lines—part B: possible commitment of regional collapse under current climate. Preprint at *Cryosphere Discuss*. https://doi.org/10.5194/tc-2022-105 (2022).
36. Urruty, B. et al. The stability of present-day Antarctic grounding lines—part A: no indication of marine ice sheet instability in the current geometry. Preprint at *Cryosphere Discuss*. https://doi.org/10.5194/tc-2022-104 (2022).
37. IPCC *Special Report on the Ocean and Cryosphere in a Changing Climate* (eds Pörtner, H.-O. et al.) (Cambridge Univ. Press, 2019).
38. IPCC *Climate Change 2021: The Physical Science Basis* (eds Masson-Delmotte et al.) (Cambridge Univ. Press, 2021).
39. Irvine, P. J., Keith, D. W. & Moore, J. Brief communication: understanding solar geoengineering's potential to limit sea level rise requires attention from cryosphere experts. *Cryosphere* **12**, 2501–2513 (2018).
40. McCusker, K. E., Battisti, D. S. & Bitz, C. M. Inability of stratospheric sulfate aerosol injections to preserve the West Antarctic Ice Sheet. *Geophys. Res. Lett.* **42**, 4989–4997 (2015).
41. Moore, J. C. et al. Greenland Ice Sheet response to stratospheric aerosol injection geoengineering. *Earths Future* **7**, 1451–1463 (2019).
42. Fettweis, X. et al. Brief communication: reduction in the future Greenland Ice Sheet surface melt with the help of solar geoengineering. *Cryosphere* **15**, 3013–3019 (2021).
43. Feldmann, J., Levermann, A. & Mengel, M. Stabilizing the West Antarctic Ice Sheet by surface mass deposition. *Sci. Adv.* **5**, eaaw4132 (2019).
44. Wolovick, M. J. & Moore, J. C. Stopping the flood: could we use targeted geoengineering to mitigate sea level rise? *Cryosphere* **12**, 2955–2967 (2018).
45. Bueler, E. & Brown, J. Shallow shelf approximation as a "sliding law" in a thermomechanically coupled ice sheet model. *J. Geophys. Res. Earth Surf.* **114**, F03008 (2009).
46. Barthel, A. et al. CMIP5 model selection for ISMIP6 ice sheet model forcing: Greenland and Antarctica. *Cryosphere* **14**, 855–879 (2020).
47. Kittel, C. et al. Diverging future surface mass balance between the Antarctic ice shelves and grounded ice sheet. *Cryosphere* **15**, 1215–1236 (2021).
48. Feldmann, J. & Levermann, A. Collapse of the West Antarctic Ice Sheet after local destabilization of the Amundsen Basin. *Proc. Natl Acad. Sci. USA* **112**, 14191–14196 (2015).
49. Martin, D. F., Cornford, S. L. & Payne, A. J. Millennial-scale vulnerability of the Antarctic Ice Sheet to regional ice shelf collapse. *Geophys. Res. Lett.* **46**, 1467–1475 (2019).
50. Sutter, J. et al. Limited retreat of the Wilkes Basin Ice Sheet during the Last Interglacial. *Geophys. Res. Lett.* **47**, e2020GL088131 (2020).
51. Lowry, D. P., Krapp, M., Golledge, N. R. & Alevropoulos-Borrill, A. The influence of emissions scenarios on future Antarctic ice loss is unlikely to emerge this century. *Commun. Earth Environ.* **2**, 221 (2021).
52. Edwards, T. L. et al. Projected land ice contributions to twenty-first-century sea level rise. *Nature* **593**, 74–82 (2021).
53. DeConto, R. M. et al. The Paris Climate Agreement and future sea-level rise from Antarctica. *Nature* **593**, 83–89 (2021).
54. The Emissions Gap Report 2022. *UNEP* https://www.unep.org/resources/emissions-gap-report-2022 (2022).
55. Garbe, J., Albrecht, T., Levermann, A., Donges, J. F. & Winkelmann, R. The hysteresis of the Antarctic Ice Sheet. *Nature* **585**, 538–544 (2020).
56. Paris Agreement. *United Nations Framework Convention on Climate Change (UNFCCC)* https://unfccc.int/sites/default/files/english_paris_agreement.pdf (2015).
57. Duffey, A., Irvine, P., Tsamados, M. & Stroeve, J. Solar geoengineering in the polar regions: a review. *Earths Future* **11**, e2023EF003679 (2023).
58. Baur, S., Nauels, A., Nicholls, Z., Sanderson, B. M., & Schleussner, C.-F. The deployment length of solar radiation modification: an interplay of mitigation, net-negative emissions and climate uncertainty. *Earth Syst. Dynam.* **14**, 367–381 (2023).
59. Morlighem, M. et al. Deep glacial troughs and stabilizing ridges unveiled beneath the margins of the Antarctic Ice Sheet. *Nat. Geosci.* **13**, 132–137 (2020).
60. Morlighem, M. 2022. *MEaSUREs BedMachine Antarctica: Bedrock Topography and Mask* Version 3 (NASA, accessed 30 May 2023); https://doi.org/10.5067/FPSU0V1MWUB6
61. Zwally, H. J., Robbins, J. W., Luthcke, S. B., Loomis, B. D. & Remy, F. Mass balance of the Antarctic Ice heet 1992–2016: reconciling results from GRACE gravimetry with ICESat, ERS1/2 and Envisat altimetry. *J. Glaciol.* **67**, 533–559 (2021).

Methods

Ice-sheet model parameterizations, set-up and resolution

To investigate the response of the AIS to a wide range of future emissions and SRM scenarios, we employ the PISM[45] with a range of parameterizations controlling ice flow and ice-shelf mass balance. Details of the spin-up of PISM to the year 1860 are given in the following. The spin-up is followed by a 145 yr common historical forcing period after which the individual ensembles are branched off in 2006 and integrated until the year CE 3000. We constrain the model ensemble by focusing on those runs that best match the recent historical record (1992–2017) of sea-level-equivalent ice volume, mass balance and annual sea-level contribution, as well as ice thickness and grounding-line positions. We employ PISM (v.1.2) in the so-called shallow shelf–shallow ice hybrid mode, which is a superposition of the shallow shelf and shallow ice approximations of the stress balance. This allows for model representation of both slow non-sliding (inland ice) and fast-flowing (glaciers) parts of the ice. To allow for 540 simulations over millennial timescales, we use a relatively coarse horizontal resolution of 16 km. The position of the grounding line is established by the flotation criterion employing a subgrid interpolation scheme[62]. Basal friction and stresses are computed accordingly. This enables a more adequate representation of grounding-line dynamics at coarse resolution. However, we repeat selected simulations on 8 and 4 km grids to assess the robustness of the respective coarse-resolution results (Extended Data Fig. 5). We note that the computation of basal melt rate at the grounding line is not affected by the subgrid interpolation but happens on the native grid. Recently, it has been suggested that seawater intrusions at the grounding line can increase melt rates locally[63]. A subgrid extrapolation of basal melt at the grounding line is one way to mimic this effect. However, it is not yet possible to quantify the increase in melt rates in situ, and a subgrid melt extrapolation almost certainly would overestimate local melt rates and bias the model to be more prone to grounding-line retreat.

In the model ensemble, we vary two parameters relevant for ice flow (Extended Data Table 1). In PISM, the till friction angle controls the yield strength in the Mohr–Coulomb criterion with low values of the till friction angle resulting in low yield strength. In our simulations, the till friction angle is linearly dependent on depth, with a maximum value of 30 and a minimum value between 3 and 8. For sliding, we employ a power law ('pseudo-plastic') with an exponent q of 0.60 or 0.75. The preceding parameters are chosen as they create a near-equilibrium ice sheet with reasonable grounding-line positions and ice cover under pre-industrial climate forcing (Supplementary Figs. 8 and 9). For a full list of parameters, see Extended Data Table 1.

Due to a lack of direct observations, basal ice-shelf melt, the major driver behind current grounding-line retreat, is highly uncertain. Therefore, we employ eight different basal ice-shelf-melt sensitivities using the Potsdam Ice-Shelf Cavity mOdel (PICO) basal shelf melt model[64,65]. Here we vary the heat exchange coefficient that controls the turbulent heat exchange from the ambient ocean across the boundary layer beneath the ice-shelf base (Extended Data Table 1). Accounting for different parameterizations of ice-sheet flow and basal friction, this amounts to 60 simulations per climate forcing and allows us to consider a wide range of potential ice-sheet responses. The sensitivity of ice-shelf melt to the heat exchange coefficient is shown in Supplementary Fig. 10. Recent observations for the Thwaites Eastern Ice Shelf[66] have shown that subshelf melt rates suggested by current regional ocean models or simplified parameterizations can considerably deviate from observations (as far as they are available). While we try to match currently estimated melt rate patterns adequately, substantial deviations from reality are to be expected.

Calving amounts to about half of the currently estimated ice-shelf mass loss[67,68]. Due to lack of a general physical fracture and melt-induced calving law, we employ a heuristic calving relationship that depends on the horizontal strain-rate field ('eigencalving'[69]). We remove all floating ice thinner than 10 m to prevent unrealistic ice-shelf geometries. Finally, we prescribe the current ice-shelf geometry as the maximum extent of floating ice to exclude unrealistic buttressing effects not in line with observations.

Historical observational ensemble constraints

We carry out a separate control simulation under constant pre-industrial forcing for each simulation and apply additional ensemble constraints on the basis of observational records. We constrain the whole model ensemble by calibration against observations of the Antarctic sea-level contribution[70], the ice-shelf mass loss due to calving and basal melting[67,68] and the present-day observed ice-mass change and grounding-line positions[61] (Supplementary Fig. 11).

Model spin-up

The model spin-up is divided into three steps with the goal to relax the ice sheet to present-day conditions. In a first step, the thermal state of the ice sheet is initiated via a 200,000 yr simulation under constant present-day forcing with a fixed ice-sheet geometry. The present-day surface climate forcing is taken from the regional climate model RACMO[71]. Subsequently, we run a 2,000 yr pre-industrial spin-up with pre-industrial climate anomalies (100 yr repeated) from HadGEM2-ES in which the ice sheet is allowed to freely evolve. These anomalies are added onto the RACMO surface mass balance and surface air temperature data and onto the World Ocean Atlas 2018 temperature and salinity fields as used in the Ice Sheet Model Intercomparison Project for CMIP6[34]. Ocean conditions are averaged between depths of 700 and 400 m, representative of the approximate depth of Antarctic ice-shelf cavities. The ensemble spread of the pre-industrial model spin-up is shown in Supplementary Fig. 9. In a last step, the model is run from 1860 until 2005 under common historical forcing from HadGEM2-ES, after which the different climate scenarios are branched off. The historical runs are restarted from a best-fit member of the pre-industrial spin-up ensemble (Supplementary Fig. 8). Note that the higher-resolution simulations (8 km and 4 km) are restarted and regridded from the 16 km pre-industrial spin-up.

Start of SRM

We consider four different starting dates for SRM under RCP 8.5 (2020, 2040, 2060 and 2080). While SRM85-20 is modelled explicitly in HadGEM2-ES, we construct the forcing for later starting dates by adding the post-2020 modelled climate anomalies of SRM85-20 onto RCP 8.5 at the years 2040, 2060 and 2080, respectively. This means we follow the RCP 8.5 scenario until the respective starting dates, upon which we continue the forcing, adding the SRM85-20 anomalies to the RCP 8.5 climate state at the year 2040, 2060 or 2080. This implies that after the start of SRM, the climate system responds similarly, regardless of whether SRM is started in the year 2020 or later during the twenty-first century. We consider this to be a reasonable assumption as the modelled twenty-first-century temperature response to RCP 8.5 remains approximately linear throughout.

Model forcing

We force PISM with anomalies (relative to pre-industrial) annual mean surface mass balance, surface air temperature, ocean temperature and salinity fields regridded from the native HadGEM2-ES-grid to the PISM-grid at 16, 8 or 4 km lateral resolution. The anomalies are added to the present-day reference field from RACMO[71] and World Ocean Data 2018[72]. The HadGEM2-ES climate projections cover the period from 1860 to 2300. To continue the climate forcing until the year CE 3000, we repeat the last 30 years (2270–2300) of the forcing until the year CE 3000. This means that we ignore natural or anthropogenic changes in atmospheric GHG concentrations and their temperature response after the year 2300.

Earth system model configuration and simulation design

HadGEM2-ES is a CMIP5-generation Earth system model (ESM) with reduced complexity compared with CMIP6-generation ESMs such as its successor, UKESM1[73]. HadGEM2-ES is a fully coupled atmosphere–ocean ESM with an atmospheric horizontal resolution of N96 (1.875° × 1.25°) and 38 vertical levels extending to 40 km altitude and an oceanic horizontal resolution of 1° (reducing to 1/3° at the Equator) with 40 vertical levels[11]. HadGEM2-ES employs the single-moment Coupled Large-scale Aerosol Simulator for Studies in Climate (CLASSIC) aerosol module, which includes a fully interactive sulfur cycle that represents sulfate in Aitken, accumulation and dissolved modes[74]. HadGEM2-ES has been utilized for many SRM studies independently and as part of GeoMIP[11,12,74], and the CLASSIC aerosol module remains in operational use for daily air quality forecasts in the United Kingdom[75]. A full description of HadGEM2-ES and its contribution to CMIP5 is provided in refs. 46,73. The design of the SRM simulations is to inject sulfur dioxide (SO_2) into the model stratosphere at such a rate as to maintain global-mean near-surface air temperature at 1.5 °C above pre-industrial levels, where the reference temperature is derived from HadGEM2-ES's 140 yr pre-industrial control simulation[15]. Three baseline GHG concentration scenarios from the CMIP5 protocol were chosen to span the range of plausible futures: the low-emissions strong-mitigation RCP 2.6, the intermediate-emissions stabilization RCP 4.5 and the high-emissions no-mitigation RCP 8.5[76,77]. Ref. 15 provides detail on how the temporally evolving SO_2 emission rates were determined for each SRM scenario, which pre-empts the online feedback algorithm used in GLENS (Geoengineering Large Ensemble Project)[8]. For the purpose of this study, the original GEO2.6 (SRM26), GEO4.5 (SRM45) and GEO8.5 (SRM85) SRM simulations were extended to the year 2300 following the RCP extension protocol outlined in ref. 71 and using the same algorithm for calculating SO_2 injection rates as described in ref. 11.

Caveats of study design

Model sensitivity. Overall, we consider our ice-sheet model set-up to have a relatively low sensitivity to climate change compared with previous studies with PISM (for example, ref. 78) and to other models currently in use (Supplementary Fig. 5)[34]. Consequently, we conclude that the modelled effectiveness (preventing ice-sheet instability) of SRM interventions shown here represents a conservative estimate with respect to ice-sheet stability (more-sensitive models would show less effectiveness of SRM). This, however, underlines our assessment that large-scale SRM interventions during the twenty-first century, if not employed early, are not sufficient to prevent WAIS collapse, assuming intermediate- or high-emissions scenarios.

Stand-alone ice-sheet model. As we run PISM in stand-alone mode (not coupled to a climate model), the climate forcing does not include feedback from ice-sheet topographic changes and freshwater hosing from ice-shelf melt/calving and surface run-off. The WAIS undergoes the most drastic elevation changes (ice-sheet collapse) until the year CE 3000; therefore, both freshwater input into the Southern Ocean and surface temperature lapse rate corrections would be largest in this area. A recent study in which ice–ocean–atmosphere feedbacks were incorporated via offline coupling of PISM to a climate model[78] suggests that the combined feedbacks accelerate ice-sheet loss in Antarctica until the year 2100. However, also in East Antarctica, where grounding-line retreat is mostly contained, surface lowering and increased ice discharge take place that might affect the magnitude of ice-sheet retreat in a coupled model set-up. In summary, it is difficult to quantify the extent to which the missing ice-to-ocean and ice-to-atmosphere feedbacks would affect ice-sheet stability.

Model resolution. We run the ice-sheet model on a relatively coarse resolution of 16 km to allow for a larger ensemble over millennial timescales. While the subgrid grounding-line interpolation is supposed to make the results more independent from model resolution, we still find different ice-sheet responses at higher resolutions of 8 and 4 km (Extended Data Figs. 4 and 5). The 8 km ice-sheet configuration at the year CE 3000 is very similar to the 16 km runs, but the pacing of retreat (onset of marine ice-sheet instability) is different. At 8 and 4 km grid resolutions, Thwaites Glacier shows a nonlinear retreat earlier compared with the 16 km simulations. However, the George V Coast grounding line bordering the Wilkes Subglacial Basin remains stable (until the year CE 3000) regardless of the resolution tested here. Taken together, this also suggests that SRM interventions would be less effective at higher resolutions, further strengthening our line of argument.

Initialization. Another issue pertaining to all ice-sheet modelling efforts is the initial configuration of the ice sheet at the beginning of the simulations. As we do not employ inversion of, for example, basal friction but rely on more general heuristics, ice-sheet thickness and grounding-line positions in critical areas are not identical to present-day observations. For example, the grounding line of Thwaites Glacier is located slightly farther upstream and WAIS surface elevation is lower than presently observed, which could favour faster retreat. Furthermore, some East Antarctic coastal regions are thicker than observations and hence more resilient to ocean warming.

Model bias in ice-shelf tributaries and surface velocities. See Supplementary Information.

Data availability

The data generated and analysed during the current study are available from the corresponding author. The data underlying the main figures are uploaded to Zenodo (https://doi.org/10.5281/zenodo.7640508) (ref. 79).

Code availability

PISM is openly available from https://github.com/pism/pism.

References

62. Feldmann, J., Albrecht, T., Khroulev, C., Pattyn, F. & Levermann, A. Resolution-dependent performance of grounding line motion in a shallow model compared with a full-Stokes model according to the MISMIP3d intercomparison. *J. Glaciol.* **60**, 353–360 (2014).
63. Robel, A. A., Wilson, E. & Seroussi, H. Layered seawater intrusion and melt under grounded ice. *Cryosphere* **16**, 451–469 (2022).
64. Reese, R., Gudmundsson, G. H., Levermann, A. & Winkelmann, R. The far reach of ice-shelf thinning in Antarctica. *Nat. Clim. Change* **8**, 53–57 (2018).
65. Reese, R., Albrecht, T., Mengel, M., Asay-Davis, X. & Winkelmann, R. Antarctic sub-shelf melt rates via PICO. *Cryosphere* **12**, 1969–1985 (2018).
66. Davis, P. E. D. et al. Suppressed basal melting in the eastern Thwaites Glacier grounding zone. *Nature* **614**, 479–485 (2023).
67. Rignot, E., Jacobs, S., Mouginot, J. & Scheuchl, B. Ice-shelf melting around Antarctica. *Science* **341**, 266–270 (2013).
68. Depoorter, M. A. et al. Calving fluxes and basal melt rates of Antarctic ice shelves. *Nature* **502**, 89–93 (2013).
69. Levermann, A. et al. Kinematic first-order calving law implies potential for abrupt ice-shelf retreat. *Cryosphere* **6**, 273–286 (2012).
70. Shepherd, A. et al. Mass balance of the Antarctic Ice Sheet from 1992 to 2017. *Nature* **558**, 219–222 (2018).
71. van Wessem, J. M. et al. Improved representation of East Antarctic surface mass balance in a regional atmospheric climate model. *J. Glaciol.* **60**, 761–770 (2014).
72. Boyer, T. P. et al. *NOAA Atlas NESDIS 87* (NOAA, 2018).
73. Sellar, A. A. et al. UKESM1: description and evaluation of the UK Earth system model. *J. Adv. Model. Earth Syst.* **11**, 4513–4558 (2019).

74. Bellouin, N. et al. Aerosol forcing in the Climate Model Intercomparison Project (CMIP5) simulations by HadGEM2-ES and the role of ammonium nitrate. *J. Geophys. Res. Atmos.* **116**, 20206 (2011).
75. Savage, N. H. et al. Air quality modelling using the Met Office Unified Model (AQUM OS24-26): model description and initial evaluation. *Geosci. Model Dev.* **6**, 353–372 (2013).
76. van Vuuren, D. P. et al. The representative concentration pathways: an overview. *Climatic Change* **109**, 5–31 (2011).
77. Meinshausen, M., Raper, S. C. B. & Wigley, T. M. L. Emulating coupled atmosphere–ocean and carbon cycle models with a simpler model, MAGICC6—part 1: model description and calibration. *Atmos. Chem. Phys.* **11**, 1417–1456 (2011).
78. Golledge, N. R. et al. Global environmental consequences of twenty-first-century ice-sheet melt. *Nature* **566**, 65–72 (2019).
79. Sutter, J. Antarctic Ice Sheet evolution under RCP and geoengineering scenarios. *Zenodo* https://doi.org/10.5281/zenodo.7640508 (2023).
80. Kittel, C. et al. Diverging future surface mass balance between the Antarctic ice shelves and grounded ice sheet. *Cryosphere* **15**, 1215–1236 (2021).

Acknowledgements

Calculations were performed on UBELIX, the high-performance computing cluster at the University of Bern. We thank G. Jansen for excellent technical support on the HPC infrastructure. J.S. acknowledges funding from the Deutsche Forschungsgemeinschaft under grant no. SU 1166/1-1. T.F.S. acknowledges funding from the Swiss National Science Foundation (grant 200020_200492) and from the European Union's Horizon 2020 research and innovation programme under grant agreement no. 820970 (project TiPES; this is TiPES contribution no. 199). T.L.F. acknowledges funding from the Swiss National Science Foundation (grant PP00P2_198897) and the European Union's Horizon 2020 research and innovation programme under grant agreement no. 820989 (project COMFORT).

Author contributions

J.S., T.F.S. and T.L.F. devised the study. J.S. set up the ice-sheet model and ran the ensemble simulations. A.J. carried out the prolonged solar radiation modification experiments. C.W. carried out the reversibility tests. J.S. analysed the ice-sheet model results T.L.F. carried out analysis on the ocean component of HadGEM2-ES. J.S. led the writing of the paper with contributions from all authors.

Competing interests

The authors declare no competing interests.

Additional information

Extended data is available for this paper at https://doi.org/10.1038/s41558-023-01738-w.

Supplementary information The online version contains supplementary material available at https://doi.org/10.1038/s41558-023-01738-w.

Correspondence and requests for materials should be addressed to J. Sutter.

Peer review information *Nature Climate Change* thanks Johannes Feldmann and the other, anonymous, reviewer(s) for their contribution to the peer review of this work.

https://doi.org/10.1038/s41558-023-01738-w

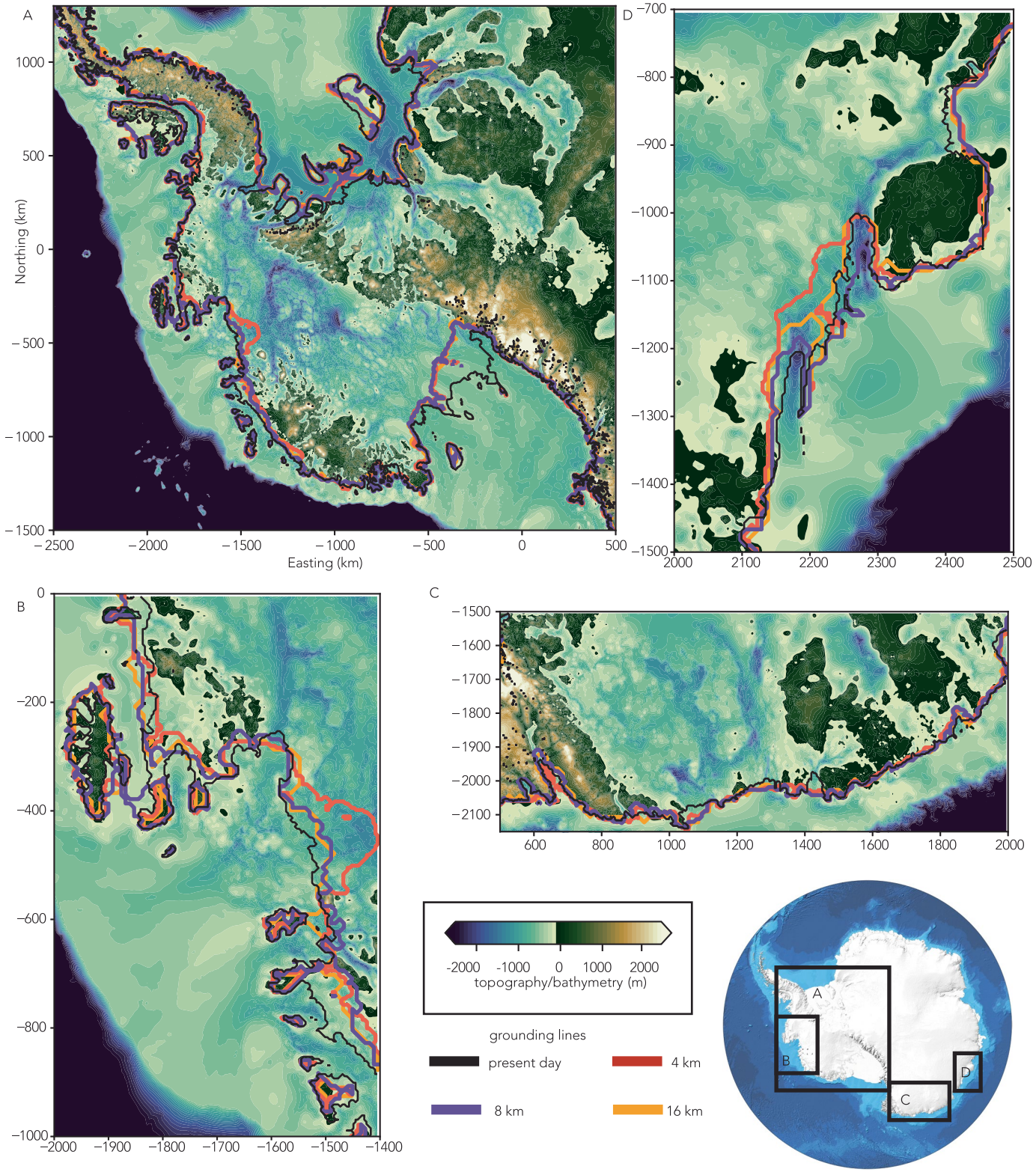

Extended Data Fig. 1 | Model resolution dependency of simulated present day grounding line position. Simulated grounding line positions at the year 2020. A) Filchner-Ronne sector, B) Amundsen Sea sector, C) George V Land D) Totten Glacier. Grounding lines at 16 km (orange line; default configuration), 8 km (green line) and 4 km (red line) resolution are displayed. Present day observed grounding line (BedMachine Antarctic, Morlighem et al. 2020) is depicted by the thin black line. Topography from Morlighem et al. 2020.

https://doi.org/10.1038/s41558-023-01738-w

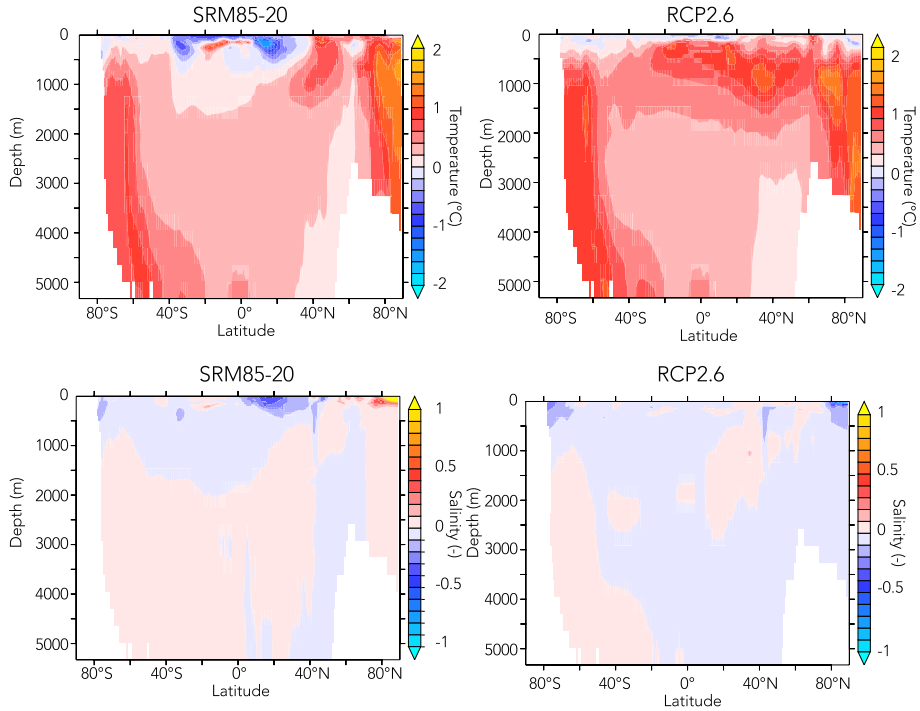

Extended Data Fig. 2 | Simulated changes in zonal mean ocean conditions under SRM scenarios. Simulated changes in zonal mean (top) temperature and (bottom) salinity in the ocean between 2021-2040 and 2281-2300 under the (left) SRM85-20 and (right) RCP2.6 scenario using HadGEM2-ES.

https://doi.org/10.1038/s41558-023-01738-w

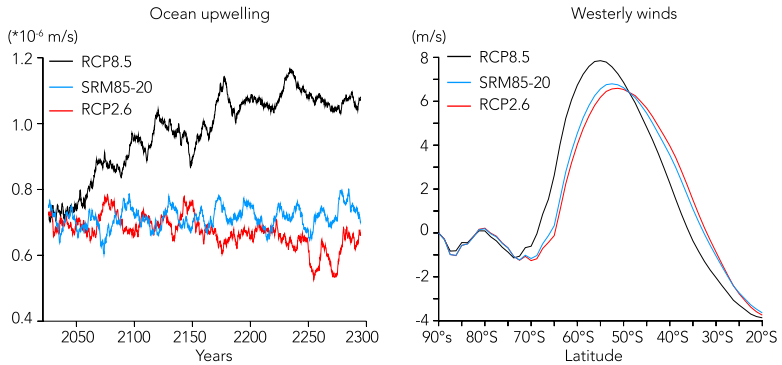

Extended Data Fig. 3 | Zonal ocean upwelling and wind stress in SRM scenario compared to RCP2.6 and RCP2.8. Left: Simulated zonal mean upwelling in the ocean averaged from 90°S to 60°S and from surface to 400 m depth for RCP8.5, RCP2.6 and SRM85-20. Timeseries are smoothed with a 10-yr running mean. Right: Simulated zonally averaged eastward component of wind at 10 m altitude for RCP8.5, RCP2.6 and SRM85-20 averaged over the period 2281-2300. Simulations are done with HadGEM2-ES.

https://doi.org/10.1038/s41558-023-01738-w

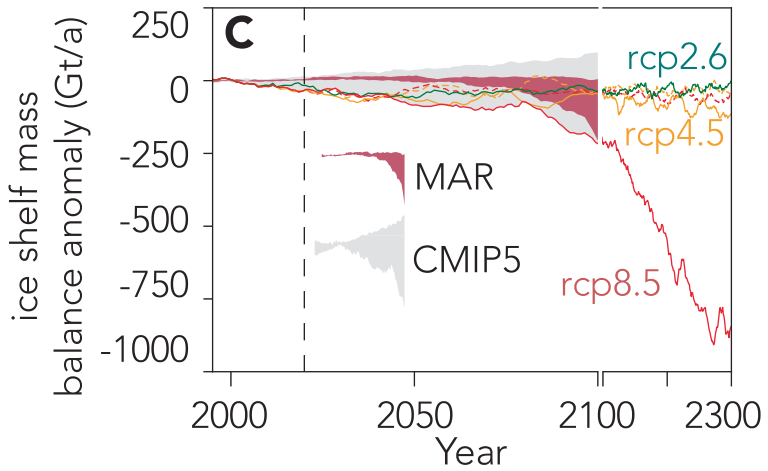

Extended Data Fig. 4 | HadGEM2-ES ice shelf mass balance. HadGEM2-ES ice shelf mass balance compared to CMIP5-range and compared to the regional climate model MAR[80].

https://doi.org/10.1038/s41558-023-01738-w

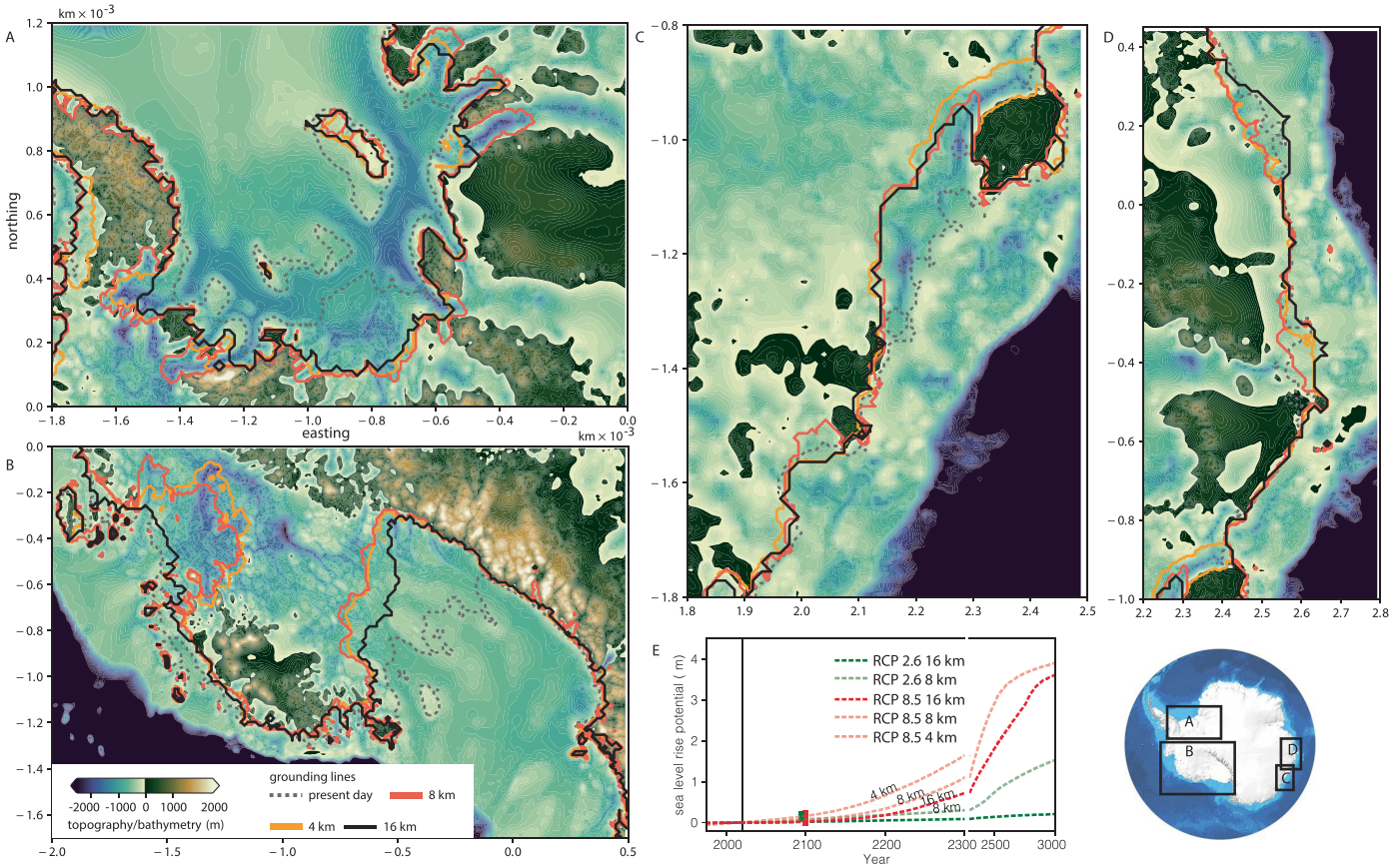

Extended Data Fig. 5 | Model resolution dependency of grounding line changes under RCP8.5 forcing at the year 2300 CE. Resolutions 4 (orange line), 8 (red line) and 16 (black line) km are displayed for A) Filchner-Ronne Ice Shelf, B) Amundsen/Ross Sea, C) Totten Glacier, D) Denman Glacier. Present day grounding line is depicted by the gray dashed line. Topography from Morlighem et al. 2020. Timeseries in E depicts sea level equivalent ice volume change in RCP2.6 and RCP8.5 depending on model resolution.

https://doi.org/10.1038/s41558-023-01738-w

Extended Data Table 1 | Scenario dependence of the future range of Antarctic sea level contributions (m) for the calibrated ensemble

Parameter	Values	Context
sia_e , ssa_e	1.0 , 1.0	Grounded and floating ice enhancement factor in flow
pQ	0.6, 0.75	Pseudo plastic sliding, power law
Φ_{min}	3,4,5,6,8	Minimum till friction angle in basal drag formulation
Φ_{max}	30	Maximum till friction angle
Topg2Φ	-700 m, 0m	Topography dependent till friction angle
γ*10^{-5}	1,2,3,4,6,8	PICO heat exchange coefficient
Eigencalving	1e17	Deviatoric stress calving law
Thickness calving	10 m	Minimum ice thickness threshold for calving

https://doi.org/10.1038/s41558-023-01738-w

Extended Data Table 2 | Selected PISM parameters used in this study

Scenario	2100 (Median)	2300 (Median)	3000 (Median)
RCP2.6	0.01 – 0.06 (0.04)	0.06 – 0.20 (0.13)	0.06 – 1.38 (0.31)
RCP4.5	-0.02 – 0.10 (0.03)	-0.01 – 0.34 (0.12)	0.06 – 1.98 (0.83)
RCP8.5	00.01 – 0.06 (0.03)	0.60 – 1.10 (0.80)	2.66 – 3.95 (3.71)
SRM85-20	-0.01 – 0.04 (0.02)	0.02 – 0.22 (0.11)	0.14 – 1.11 (0.53)
SRM45-20	-0.02 – 0.07 (0.01)	-0.02 – 0.32 (0.08)	-0.09 – 1.07 (0.30)
SRM85-40	0.0 – 0.06 (0.03)	0.05 – 0.27 (0.14)	0.3 – 1.75 (0.91)
SRM45-40	-0.02 – 0.09 (0.02)	0.0 – 0.33 (0.1)	-0.03 – 1.46 (0.37)
SRM85-60	0.01 – 0.06 (0.03)	0.07 – 0.26 (0.15)	0.56 – 1.89 (0.87)
SRM45-60	-0.02 – 0.10 (0.02)	0.01 – 0.31 (0.11)	0.06 – 1.65 (0.62)
SRM85-80	0.0 – 0.06 (0.02)	0.06 – 0.26 (0.15)	0.44 – 2.16 (1.65)
SRM45-80	-0.02 – 0.10 (0.02)	0.01 – 0.33 (0.12)	0.13 – 2.05 (0.82)